small NANO MICRO

Nanotubes

Tube-in-Tube TiO_2 Nanotubes with Porous Walls: Fabrication, Formation Mechanism, and Photocatalytic Properties

Xijin Xu, Xiaosheng Fang, Tianyou Zhai,* Haibo Zeng,* Baodan Liu, Xiaoye Hu, Yoshio Bando, and Dmitri Golberg**

Since the identification of carbon nanotubes by Iijima in 1991,[1] 1D nanoscale structures have attracted substantial scientific and technological interest. In the following years, the chemical syntheses of various noncarbon nanotubes, in particular transition metal oxide nanotubes such as titanium dioxide (TiO_2) nanotubes, was performed.[2,3] TiO_2 has attracted a lot of interest because of its unique photoinduced reactivity explored for applications in environmental photocatalysis,[4,5] solar energy conversion,[6] and light-induced amphiphilicity.[7] Many methods, such as anodization,[8] template techniques,[9,10] hydrothermal processes,[11,12] and soft chemical processes[13] have been used to prepare TiO_2 nanotubes. Among the fabrication techniques, the electrochemical anodization process, since its discovery, has become very useful in producing high-aspect-ratio nanotubes with a controllable pore size and morphology.[14,15] Furthermore, using this simple, cheap and straightforward method, TiO_2 nanotube arrays self-aligned as they grew during anodization of Ti.[16] The tube lengths can be in the range from a few micrometers to several hundreds of micrometers and their diameters vary from 10 to 200 nm.[17–20] These self-organized TiO_2 nanotubes can be attached to a Ti substrate or suspended as membranes,[21] that then may be used for the fabrication of other nanomaterials. However, traditional TiO_2 nanotube arrays fabricated in the previous works exhibited standard one-wall structure, and the walls of such nanotubes were compact. The most important application of TiO_2 nanotube arrays is in the photoelectrochemistry field, such as environmental pollutant degradation, water splitting, and photoelectric conversion.[22–24] These properties are strongly related to the surface area and local microstructure of nanotubes, such as porosity of walls and two- or many-wall structures. For the latter types of tubular structures, a larger contact surface area may be achieved due to the multiwalled morphologies compared with standard one-wall nanotubes. Therefore, adjustment of the microstructure inside a tube wall has become an attractive and challenging topic.

Herein it is shown that tube-in-tube (TIT) TiO_2 nanostructures with coarse, porous walls can be obtained. This greatly increases the surface area of the nanostructures. In addition, three structure domains, namely, the internal and external tube surfaces together with the areas between the two coarse subshells within the tube, all become available for reactions. This improves the tube's photocatalytic properties. Furthermore, the effects of crystallinity on the photocatalysis and the formation mechanism of these novel unusual nanostructures are discussed.

TIT TiO_2 nanotube parallel arrays were arranged perpendicularly to the substrate surfaces (see Experimental Section for details). It should be noted that the formation of highly ordered TiO_2 nanotubes with one wall was reported previously.[25] **Figure 1** shows that the present TIT TiO_2 nanostructures cover the entire substrate surface. The enlarged scanning electron microscopy (SEM) images (Figure 1b,c) clearly show numerous TIT TiO_2 nanotubelike structures. These arrays are uniform and compact, at least several micrometers in length (Figure 1a), and the outer tube diameter within the array is ≈200 nm (Figure 1b,c). The nanotubes possess a coarse lateral profile (Figure 1d), have a larger contact surface area compared to conventional structures, and may be good for photocatalytic applications.

The thermal annealing process of the as-prepared arrays was carried out at 550 °C in air for 3 h for the entire nanotube array crystallization. The corresponding X-ray diffractometry (XRD) patterns, recorded from the as-grown and annealed TIT nanostructures, are shown in **Figure 2**a.

Dr. X. J. Xu, Dr. X. S. Fang, Dr. T. Y. Zhai, Dr. H. B. Zeng, Dr. B. D. Liu, Prof. Y. Bando, Prof. D. Golberg
International Center for Young Scientists (ICYS) and International Center for Materials Nanoarchitectonics (MANA)
National Institute for Materials Science (NIMS)
Namiki 1–1, Tsukuba, Ibaraki 305–0044, Japan
E-mail: x.xu@griffith.edu.au, xijinxu@yahoo.cn; zhai.tianyou@gmail.com; zeng.haibo@nims.go.jp; GOLBERG.Dmitri@nims.go.jp

Dr. X. J. Xu
Environmental Futures Centre and Griffith School of Environment
Gold Coast Campus
Griffith University
QLD 4222, Australia

Dr. X. Y. Hu
Key Laboratory of Materials Physics and Anhui Key Laboratory of Nanomaterials and Nanostructures
Institute of Solid State Physics
Chinese Academy of Sciences
P.O. Box 1129, Hefei 230031, China

DOI: 10.1002/smll.201001849

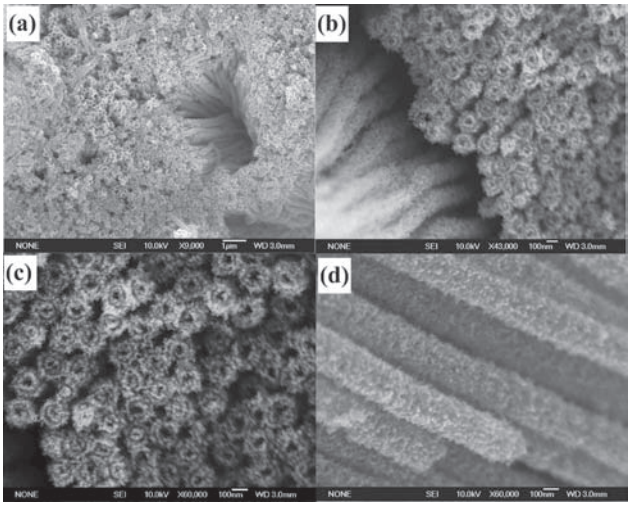

Figure 1. SEM images of TIT TiO_2 nanostructures at a low magnification (a,b), and the corresponding enlarged top-view image (c) and side-view image (d).

It can be seen that the TIT nanostructures are amorphous before annealing and the crystallinity is rather poor (bottom curve in Figure 2a). The peaks for the as-prepared sample are only due to a Ti substrate foil. After the heat treatment, the nanostructures crystallize in an anatase phase, as confirmed by the sharper X-ray peaks which appear (top curve in Figure 2a). The results are further confirmed by Raman spectroscopy (Figure 2b). The broad spectrum ranging from 100 to 1000 cm^{-1} is peculiar to the as-prepared sample (amorphous curve in Figure 2b). When the samples are annealed, the Raman spectrum (anatase curve in Figure 2b) shows the characteristic peaks of the anatase TiO_2 phase at 145, 198, 399, 516, and 640 cm^{-1}.[26,27] It is known that such a phase is preferable with respect to the photoactivity[28] of the TiO_2 nanotubes in dye-sensitized solar cells.

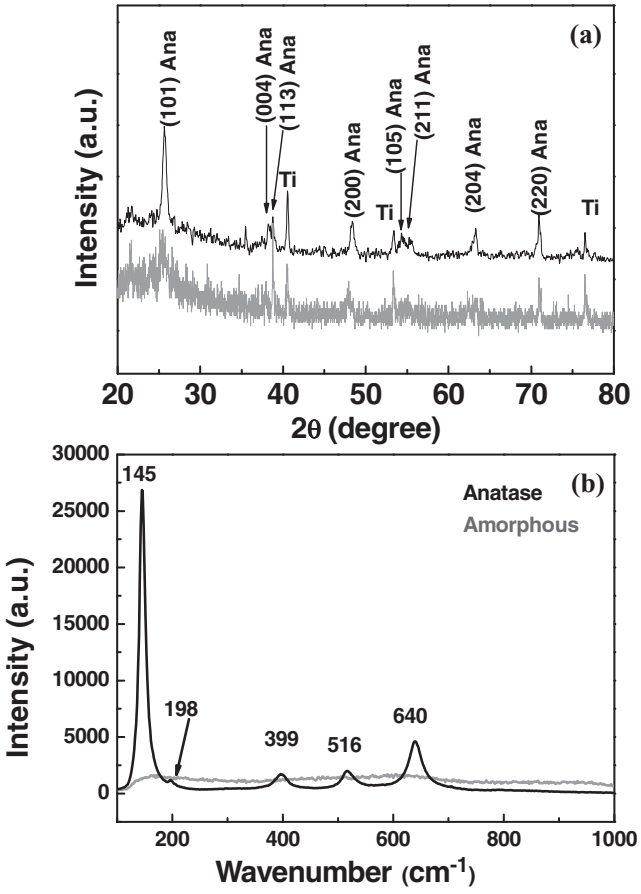

Figure 2. XRD patterns (a) and Raman spectra (b) of amorphous (red curve) and anatase (black curve) TIT TiO_2 nanostructures.

Transmission electron microscopy (TEM) and high-resolution TEM (HRTEM) images of the products are displayed in **Figure 3** for the as-grown and annealed TIT nanostructures. They show that the nanostructures have uniform diameters throughout their lengths. The TIT morphologies are preserved after the thermal treatment. Looking at Figure 3a,c, one can see that the tubes are composed of some rodlike structures. An HRTEM image (Figure 3b) shows that they are amorphous. Compared with the as-grown TIT nanostructures, the annealed samples become mainly anatase single-crystals. The lattice fringes are separated by ca 0.24 nm (Figure 3e), in accordance with the [004] zone axis pattern of an anatase TiO_2 crystal (JCPDS card No. 02–0406). The corresponding FFT pattern (inset of Figure 3e) can be indexed to the (004) diffraction planes of the anatase hexagonal structure, in accordance with the HRTEM results. A detailed chemical analysis of the arrays was carried out using energy dispersive X-ray spectroscopy (EDS). The EDS analysis (overlay Figure 3c) clearly shows that the TIT TiO_2 nanostructures are composed of Ti and O (the Cu signals come from the copper TEM grid). The composition ratio is close to Ti:O ≈ 1:2. The elemental maps displayed in the Supporting Information (SI), Figure S1 shed the light on the distribution of the constituent elements. The corresponding line profiles across the maps are also shown in Figure 3f. In SI, Figure S1, the Ti K-edge and the O K-edge intensities are evenly distributed throughout the structure with a depleting signal at the intervals between the inner and outer tubes. The line profiles (SI, Figure S2 indicates the scanning direction across the nanostructure) further confirm the TIT morphology.

Titanium dioxide is one of the most popular photocatalytic materials able to degrade pollutants under both UV and visible light illumination, when combined with a dopant such as methylene blue (MB),[29–32] gaseous toluene,[33] methyl orange,[34,35] amaranth,[36] and phenol.[37] Due to the specific ordering within the TIT nanostructures, high photocatalytic efficiency is expected. The uniform interfacial structure between the two shells of TiO_2 is absent in standard one-walled TiO_2 nanotubes. The photocatalytic activities of the samples were evaluated by measuring the degradation of MB in an aqueous solution under UV light irradiation. **Figure 4** shows the effects of annealing on the photocatalytic degradation of MB for the TIT TiO_2 nanostructures. The results verify that the photocatalytic activities increase when the TIT nanostructures have been annealed, i.e., the crystalline nanotubes have a stronger photocatalytic activity than the amorphous samples. In a photocatalytic reaction,

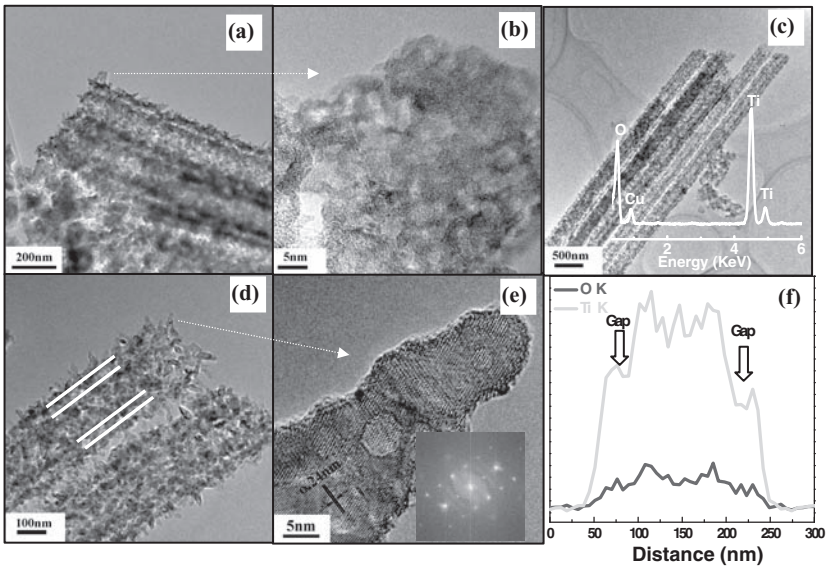

Figure 3. a) TEM image, b) HRTEM image for the as-grown TIT TiO_2 nanostructures; c,d) TEM images and e) HRTEM image and corresponding FFT pattern (e inset) and EDS spectrum of the annealed nanostructures (c overlay); f) The EDS line scanning profiles across the maps. The lowered parts labeled by arrows indicate the spatial gaps between the outer and inner tubes.

the anatase phase and surface area are the most important criteria.[38–40] When the nanotubes are annealed, the amorphous TiO_2 gradually turns into anatase TiO_2 and such crystallization raises the photocatalytic activity. In addition to the effects of crystallinity, the effects of morphologies on the photocatalytic degradation of MB on the TiO_2 nanotubes were also studied. While comparing the present TIT nanostructures with as-prepared standard one-walled TiO_2 tubes (SI, Figures S3 and S4) it can be seen that the new structures have also a stronger and faster photocatalytic response than the conventional tubes, no matter whether the crystalline or amorphous phase is considered. Furthermore, compared with the one-walled TiO_2 nanotubes reported,[32] the decomposition rate on TIT TiO_2 nanostructures is also faster. When the irradiation time was 180 min, the ratios of the concentrations between the current and primal solutions (C/C_0) decomposed by TIT TiO_2 nanostructures were 0.48 and 0.23, respectively, all smaller than that of the one-walled nanotubes (0.66).[32] This meant that more dopants had been decomposed by TIT TiO_2 nanostructures under the same irradiation time, indicating a better photocatalytic performance of the TIT-structured TiO_2 compared with normal one-walled TiO_2 nanotubes.

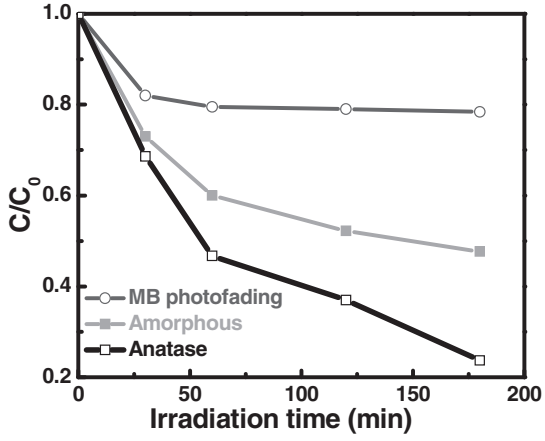

Figure 4. Photodegradation efficiency of MB by the TIT TiO_2 nanotubes for amorphous and anatase phase nanostructures.

Chemical reactions during Ti anodization are complex. They have been investigated by several groups.[41–43] Besides the usual TiO_2 nanotube with smooth one-walled morphology, many different morphologies such as dotlike structures, nanopowders consisting of granules, single nanopowders, coexistence of nanopowder and nanotubes, and nanowires were also realized by adjusting experimental conditions such as the electrolyte or applied voltage.[44,47,48] It is commonly accepted that the formation process of TiO_2 nanotubes includes field-assisted oxidation of a Ti metal to form TiO_2, field-assisted dissolution of Ti metal ions in an electrolyte and chemical dissolution of Ti and TiO_2 due to etching by fluoride ions[25] and hydrogen ions.[44] The competition between dissolution of oxide at the oxide/electrolyte interface and oxidation of the metal at the oxide/metal interface governs the formation and length of the nanotubes, and localized acidification affects their morphology. The formation mechanism of TIT TiO_2 nanotubes with porous walls can be described based on the equal-field strength model[41] together with the localized dissolution of the formed TiO_2 tubular walls.

When Ti is anodized, a barrier layer of TiO_2 forms on the metal surface. The initiation of pore formation is caused due to the defects and the rough surface in a barrier layer.[45] When a pore is developed from a surface pit, at the electrolyte/oxide interface in the early stage of the anodization (see SI, Figure S5a), TiO_2 is dissolved in the fluoride anion-containing electrolyte. This process reduces the thickness of the oxide layer and the hydrogen fluoride is consumed, which is the key to controlling the surface morphology. The oxygen anions also migrate from the electrolyte/oxide interface to the oxide/Ti interface to form Ti oxide or Ti hydroxide. However, a large amount of oxygen anions is still needed to build the walls of the pores, and these anions come from the dissociation of water. Consequently, the reaction at the electrolyte/oxide interface can be written as:

$$TiO_2 + nH_2O + 6F^- \rightarrow [TiF_6]^{2-} + (n + 2 - x)O^{2-} + xOH^- + (2n - x)H^+ \quad (1)$$

where $[TiF_6]^{2-}$ are anions dissolved into the electrolyte. The oxygen anions migrate in the electric field from the solid surface to the hydroxide/metal interface, contributing to the formation of the oxide/hydroxide layer. The hydroxide at the oxide/hydroxide interface continuously decomposes to form titanium oxide. The thicknesses of both the oxide and

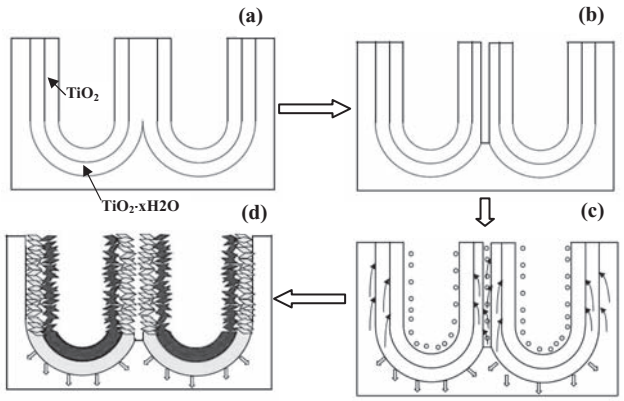

Figure 5. Schematic drawing of the TIT TiO_2 nanostructure formation process. a) The expansion stops when two nanotubes touch each other. b) The hydroxide layer between these nanotubes shrinks along the side surfaces. c) The electric field-directed chemical etching processes of the nanotubes by the hydrogen and fluoride ions. The black arrows show the direction of the electric field lines. d) The formation of final TIT TiO_2 nanostructures.

hydroxide layers are constant under certain anodization conditions in a steady state. The overall oxidation reaction can be expressed as:

$$2Ti + 2O^{2-} + 4OH^- \rightarrow TiO_2 + Ti(OH)_4 + 8e^- \quad (2)$$

Equation (2) leads to an increase in the thickness of the oxide layer. O^{2-} and OH^- anions migrate from the TiO_2/electrolyte interface to the TiO_2/Ti interface to oxidize Ti, forming a layer of titanium oxide hydroxide. While the oxidation process continues at the hydroxide/metal interface, the hydroxide at the oxide/hydroxide interface is dehydrated to TiO_2. This fact was also confirmed by Taveira et al. using X-ray photoelectron spectroscopy (XPS) in the compact layer formed at the early stage[46] and Su et al.[43] during the anodization of titanium. The authors also confirmed that the two-layer structure was formed. The outer layer was more likely to be some type of titanium hydroxide with a lower relative density, while the inner layer was titanium oxide. So there exist three interfaces, which are, namely, the solution/hydroxide interface, oxide/hydroxide interface and oxide/metal interface.

In addition to the growth of one nanotube at the bottom (downwards), the pore diameter also expands until two nanotubes touch each other, as shown in **Figure 5**a (as shown in SI, Figure S5b,c), then the expansion stops. The hydroxide layer can shrink along the directions perpendicular to the side surfaces of the nanotubes, forming separated nanotubes with two layer walls (Figure 5b). Since the thickness of the wall is determined by the anodization conditions (mainly the field strength) and the movement of the nanotube walls towards each other (driven by the self-enlargement potential), the process eventually results in a shift of the nanotubes.

When the nanotubes are separated, the hydrogen ions and fluoride ions penetrate into the intervals between the two tubes and into the pores, as shown in Figure 5c and SI, Figure S5d. According to the previous report devoted to the fabrication of TiO_2 nanowires by Choi et al.,[44] the surface morphology of porous TiO_2 nanostructures is distinctly changed as a function of anodizing time. This coincides with the fact that in our experimental process there is dissolution of the TiO_2 layer due to the effects of hydrogen and fluoride ions in the solution (Figure 5c). And as the time of the anodization process prolongs, the walls of the nanotubes become finally split off under electric-field-directed (electro) chemical etching by hydrogen and fluoride ions. The collective effects of the electrolyte components, the anodization time and the applied voltage during anodization lead to the formation of the resultant TiO_2 nanotubes with tube-in-tube morphology over the entire arrays (Figure 5d, and SI, Figure S5e,f).

In summary, we have demonstrated the formation of self-organized, freestanding TIT TiO_2 nanotubes using a one-step anodic method. It is additionally shown that the as-grown TIT TiO_2 nanostructures are amorphous, but transform into photoactive anatase phase after annealing at 550 °C in air, as verified by Raman spectroscopy. For the formation mechanism of TIT TiO_2 nanotubes with porous walls we propose that the equal-field strength growth together with the localized dissolution of the formed TiO_2 tubular walls play the key roles and dominate the formation of this novel morphology. The analysis of photocatalytic activity shows that anatase TIT TiO_2 nanostructures have better photocatalytic properties compared with their amorphous counterparts. The larger contact surface area due to the porous walls of the present new structures gives a clear advantage in environmental photocatalysis and solar energy conversion applications.

Experimental Section

TiO_2 nanotube arrays were grown on a Ti foil. Briefly, a Ti foil (Sigma-Aldrich; 250 μm thick, 99.7% purity) was cut into a 2.5 cm × 1.0 cm piece. It was degreased by ultrasonication for 30 min in acetone, followed by a thorough rinse with DI water. The mixture of 2% HF and DMSO was used as the electrolyte. Electrochemical anodization of the Ti foil was performed in a two electrode cell at room temperature using a DC power supply, for which a Pt foil was used as the counter electrode. Anodization was conducted at a constant potential of 40 V for 48 h. After anodization, the Ti foil with the TiO_2 nanotubes grown on one side of its surfaces was thoroughly washed with a large amount of DI water and acetone. After the fabrication an annealing process was applied to transform the TiO_2 nanotubes from amorphous to anatase phase. Thermal treatments of the nanotube layers were carried out in air, and the temperature was increased to 550 °C from room temperature in 2 h, then kept for 3 h. Finally, the specimens were cooled to room temperature.

The synthesized products were characterized by an SEM, (JSM-6700F), an HRTEM (JEM-3000F) equipped with an EDS, an XRD (Shimadzu 6000 X-ray diffractometer, Cu K radiation, $\lambda = 1.5406$ Å) and a Raman spectrometer (Raman, Horiba Jobin-Yoon T6400). After structure characterizations the photocatalytic properties were studied. For the photocatalytic activity evaluation the concentration of photodegrated MB was recorded by a spectrophotometer (SP-2000UV). The organic dyes (primal solution: 1.0×10^{-5} M, 30 mL) and the catalysts (10 mg) were thoroughly stirred in the dark to reach the adsorption equilibrium of the organic dyes with

small NANO MICRO

the catalyst and then exposed to UV light (125 W, 250 nm). The distance between the light source and the specimen was about 10 cm, and we tested the concentration of the solution every 30–60 min.

Supporting Information

Supporting Information is available from the Wiley Online Library or from the author.

Acknowledgements

This work was supported by the International Center for Materials Nanoarchitectonics (MANA), MEXT, Japan. H. B. Zeng thanks the Japan Society for Promotion of Science (JSPS) for a support in the form of a fellowship tenable at the National Institute for Materials Science (NIMS), Tsukuba, Japan.

[1] S. Iijima, *Nature* **1991**, *354*, 56.
[2] P. Hoyer, *Adv. Mater.* **1996**, *8*, 857.
[3] T. Kasuga, M. Hiramatsu, A. Hoson, T. Sekino, K. Niihara, *Langmuir* **1998**, *14*, 3160.
[4] K. Hashimoto, H. Irie, A. Fujishima, *Jpn. J. Appl. Phys.* **2005**, *44*, 8269.
[5] H. Choi, A. C. Sofranko, D. D. Dionysiou, *Adv. Funct. Mater.* **2006**, *16*, 1067.
[6] M. Grätzel, *Nature* **2001**, *414*, 338.
[7] R. Wang, K. Hashimoto, A. Fujishima, M. Chikuni, E. Kojima, A. Kitamura, M. Shimhigoshi, T. Watanabe, *Nature* **1997**, *388*, 431.
[8] Q. Cai, L. Yang, Y. Yu, *Thin Solid Films* **2006**, *515*, 1802.
[9] J. Qiu, Z. Jin, Z. Liu, X. Liu, G. Liu, W. Wu, X. Zhang, X. Gao, *Thin Solid Films* **2007**, *515*, 2897.
[10] M. S. Sander, M. J. Côté, W. Gu, B. M. Kile, C. P. Tripp, *Adv. Mater.* **2004**, *16*, 2052.
[11] H. Zhang, G. R. Li, L. P. An, T. Y. Yan, X. P. Gao, H. Y. Zhu, *J. Phys. Chem. C* **2007**, *111*, 6143.
[12] L. Q. Weng, S. H. Song, S. Hodgson, A. Baker, J. Yu, *J. Eur. Ceram. Soc.* **2006**, *26*, 1405.
[13] M. Wei, H. Zhou, Y. Konishi, M. Ichihara, H. Sugiha, H. Arakawa, *Inorg. Chem.* **2006**, *45*, 5684.
[14] V. Zwilling, E. Darque-Ceretti, A. Boutry-Forveille, D. David, M. Y. Perrin, M. Aucouturier, *Surf. Interface Anal.* **1999**, *27*, 629.
[15] D. Gong, C. A. Grimes, O. K. Varghese, W. Hu, R. S. Singh, Z. Chen, E. C. Dickey, *J. Mater. Res.* **2001**, *16*, 3331.
[16] V. Zwilling, M. Aucouturier, E. Darque-Ceretti, *Electrochim. Acta* **1999**, *45*, 921.
[17] S. P. Albu, A. Ghicov, J. M. Macak, P. Schmuki, *Phys. St. Sol.* **2007**, *1*, R65.
[18] J. M. Macak, H. Tsuchiya, P. Schmuki, *Angew. Chem. Int. Ed.* **2005**, *44*, 2100.
[19] D. J. Yang, H. Park, H. G. Kim, S. J. Cho, W. Y. Choi, *J. Electroceram.* **2009**, *23*, 159.
[20] S. Bauer, S. Kleber, P. Schmuki, *Electrochem. Commun.* **2006**, *8*, 1321.
[21] S. P. Albu, A. Ghicov, J. M. Macak, R. Hahn, P. Schmuki, *Nano Lett.* **2007**, *7*, 1286.
[22] H. Zeng, W. Cai, P. Liu, X. Xu, H. Zhou, C. Klingshirn, H. Kalt, *ACS Nano* **2008**, *2*, 1661.
[23] L. Kavan, M. Grätzel, S. E. Gilbert, C. Klemenz, H. J. Scheel, *J. Am. Chem. Soc.* **1996**, *118*, 6716.
[24] W. H. Leng, H. Liu, S. A. Cheng, J. Q. Zhang, C. N. Cao, *J. Photochem. Photobiol. A* **2000**, *131*, 125.
[25] M. Paulose, K. Shankar, S. Yoriya, H. E. Prakasam, O. K. Varghese, G. K. Mor, T. A. Latempa, A. Fitzgerald, C. A. Grimes, *J. Phys. Chem. B* **2006**, *110*, 16179.
[26] O. K. Varghese, D. W. Gong, M. Paulose, K. G. Ong, E. C. Dickey, C. A. Grimes, *Adv. Mater.* **2003**, *15*, 624.
[27] J. Wang, Z. Lin, *Chem. Mater.* **2008**, *20*, 1257.
[28] K. Varghese, D. W. Gong, M. Paulose, C. A. Grimes, E. C. Dickey, *J. Mater. Res.* **2003**, *18*, 156.
[29] D. Gu, Y. Lu, B. Yang, Y. Hu, *Chem. Commun.* **2008**, 2453.
[30] C. Lin, W. Yu, Y. Lu, S. Chien, *Chem. Commun.* **2008**, 6031.
[31] Zhang, J. H. Pan, A. J. Du, P. F. Lee, D. D. Sun, J. O. Leckie, *Chem. Lett.* **2008**, *37*, 424.
[32] D. Wang, T. Hu, L. Hu, B. Yu, Y. Xia, F. Zhou, W. Liu, *Adv. Funct. Mater.* **2009**, *19*, 1930.
[33] Z. Wu, F. Dong, W. Zhao, H. Wang, Y. Liu, B. Guan, *Nanotechnology* **2009**, *20*, 235701.
[34] L. Yang, S. Luo, S. Liu, Q. Cai, *J. Phys. Chem. C* **2008**, *112*, 8939.
[35] D. N. Tafen, J. Wang, N. Wu, J. P. Lewis, *Appl. Phys. Lett.* **2009**, *94*, 093101.
[36] M. Qamar, S. J. Kim, A. K. Ganguli, *Nanotechnology* **2009**, *20*, 455703.
[37] Y. Wu, M. Long, W. Cai, S. Dai, C. Chen, D. Wu, J. Bai, *Nanotechnology* **2009**, *20*, 185703.
[38] Y. Wang, Y. Meng, H. Ding, Y. Shan, X. Zhao, X. Tang, *J. Phys. Chem. C* **2008**, *112*, 6620.
[39] H. An, B. Zhu, J. Li, J. Zhou, S. Wang, S. Zhang, S. Wu, W. Huang, *J. Phys. Chem. C* **2008**, *112*, 18772.
[40] J. Wang, R. H. Li, Z. H. Zhang, X. D. Zhang, W. Sun, H. Wang, R. Xu, Z. Q. Xing, *J. Chem. Technol. Biotechnol.* **2007**, *82*, 588.
[41] Z. Su, W. Zhou, *J. Mater. Chem.* **2009**, *19*, 2301.
[42] G. K. Mor, O. K. Varghese, M. Paulose, N. Mukherjee, C. A. Grimes, *J. Mater. Res.* **2003**, *18*, 2588.
[43] Z. Su, W. Zhou, *Adv. Mater.* **2008**, *20*, 3663.
[44] J. H. Lim, J. Choi, *Small* **2007**, *3*, 1504.
[45] Z. X. Su, G. Hahner, W. Z. Zhou, *J. Mater. Chem.* **2008**, *18*, 5787.
[46] L. V. Taveira, J. M. Macak, H. Tsuchiya, L. F. P. Dick, P. Schmuki, *J. Electrochem. Soc.* **2005**, *152*, B405.
[47] S. E. Kim, J. H. Lim, S. C. Lee, S. C. Nam, H. G. Kang, J. Choi, *Electrochim. Acta* **2008**, *53*, 4846.
[48] J. Choi, R. B. Wehrspohn, J. Lee, U. Gösele, *Electrochim. Acta* **2004**, *49*, 2645.

Received: October 19, 2010
Revised: November 19, 2010
Published online: December 27, 2010

